Chemistry—Methods

Research Article
doi.org/10.1002/cmtd.202500124

Chemistry Europe
European Chemical Societies Publishing

www.chemistrymethods.org

Functionalized Donor–π–Acceptor (D–π–A) Organic Linkers for Metal–Organic Frameworks with Extended Visible-Light Absorption

Giorgia Salerno, Claudia Favia, Aurelia Falcicchio, Rocco Caliandro, Norberto Manfredi, Alessandro Abbotto, and Ottavia Bettucci*

Metal–organic frameworks (MOFs) are promising materials for photocatalytic hydrogen production. However, their efficiency is often limited by the optical properties of conventional organic linkers, such as terephthalic acid (TA). In this work, the synthesis of two novel triphenylamine-based organic dyes (L0-TA and L1-TA) featuring a donor–π–acceptor (D–π–A) structure is reported. These dyes are functionalized with a terminal moiety analogous to aminoterephthalic acid, which serves as visible-light-absorbing linkers. These dyes retain the coordination ability required for MOF assembly while enhancing light-harvesting properties. Crystallographic simulations confirm the structural compatibility of these colinkers in hybrid MOFs, providing a viable strategy to maintain MOF crystallinity while improving photocatalytic performance.

1. Introduction

Metal–organic frameworks (MOFs) are an emerging class of crystalline porous materials built via coordination of metal ions or clusters with organic linkers.[1,2] Due to their high surface area, tunable pore sizes, and versatile chemical functionalities, MOFs have shown great potential in a wide range of applications, including gas storage, separation, sensing, and catalysis.[3–9] Among these, their potential as photocatalysts in several fields, especially in hydrogen production through water splitting, has attracted growing interest over the last decade.[10–13]

The photocatalytic performance of MOFs strongly depends on the electronic properties and light absorption capabilities of the organic linkers comprising their framework. Conventional linkers, such as terephthalic acid (TA) and its amino derivatives, are well-established building blocks that confer structural stability but often limit visible-(vis)light absorption, which is critical for solar-driven catalysis.[14–16] To overcome this limitation, recent studies have explored the design of novel linkers with extended π-conjugation and tailored functional groups to enhance vis-light harvesting and charge transfer efficiency.[17]

In this context, postsynthetic modification of free functional groups of MOFs is an explored strategy to improve the light-harvesting properties of the MOFs.[18–22] In particular, the amino group of the commonly used MOF NH_2MIL125 could be a relevant functionalization strategy to improve light absorption and photocatalytic activity in MOFs.[12,23–25] However, problems related to the quantification of the functionalization rate, as well as the complexity of functionalizing the resulting material, remain significant. For this reason, the synthesis of new linkers that combine the favorable structural features of aminoterephthalic acid with additional chromophore or electron-rich moieties remains a compelling approach to further push the boundaries of MOF-based photocatalysts.

The use of chromophores is widespread in catalysis and photocatalysis, where they play a key role in enhancing reaction efficiency.[26–29] However, an unexplored and promising strategy may involve the use of organic dyes as potential linkers in MOF structures. As potential chromophores, dyes with a D–π–A architecture represent an interesting option due to their high variability, low cost, high electron transfer efficiency, and good photochemical stability.[30–32] These molecules, already employed in fields such as dye-sensitized solar cells and photocatalytic hydrogen generation,[15,33–35] have demonstrated strong vis-light absorption and efficient intramolecular charge transfer (ICT) properties, making them attractive candidates for integration into MOF structures to enhance solar light harvesting and, in turn, photocatalytic performance.

In this work, the synthesis of two novel triphenylamine-based dyes, **L0-TA** and **L1-TA** (**Figure 1**), featuring a terminal moiety structurally analogous to aminoterephthalic acid, is reported. These dyes were designed to absorb strongly in the Vis range and serve as organic linkers for MOF synthesis, retaining the robust coordination chemistry typical of TA, essential for effective MOF assembly, while

G. Salerno, N. Manfredi, A. Abbotto, O. Bettucci
Department of Materials Science
Solar Energy Research Center MIB-SOLAR and INSTM Milano-Bicocca
Research Unit University of Milano-Bicocca
Via Cozzi 55, I-20125 Milano, Italy
E-mail: ottavia.bettucci@unimib.it

C. Favia, A. Falcicchio, R. Caliandro
Institute of Crystallography
National Research Council of Italy
via Amendola 122/o, I-70126 Bari, Italy

Supporting information for this article is available on the WWW under https://doi.org/10.1002/cmtd.202500124

Research Article
doi.org/10.1002/cmtd.202500124
Chemistry Europe
European Chemical Societies Publishing

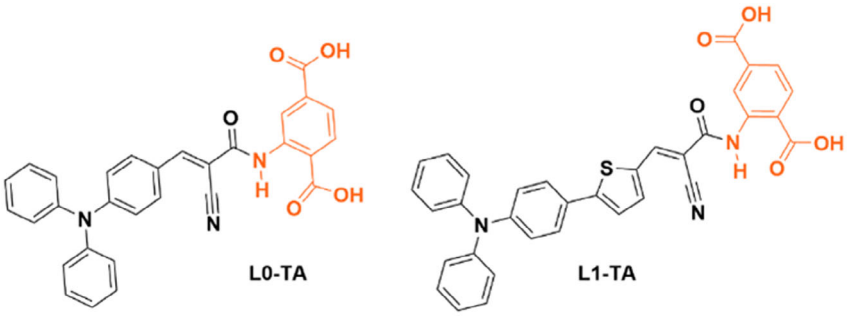

Figure 1. Structure of the novel dyes, **L0-TA** and **L1-TA**, synthesized in this work.

introducing enhanced photophysical properties to improve light harvesting and hydrogen evolution performance. Successful incorporation of these linkers into MOFs is expected to contribute to the development of more efficient, vis-light–active photocatalysts.

Although the relatively large size and steric bulk of these dyes may hinder the formation of highly crystalline MOFs when used as sole linkers, their implementation as colinkers in hybrid MOFs represents a promising alternative. Indeed, **L0-TA** and **L1-TA** can be combined with conventional linkers, such as TA, to maintain structural order while enhancing light-harvesting capabilities and photocatalytic efficiency. Crystallographic simulations support their potential integration into MOFs, confirming that the molecular dimensions and coordination geometry of both dyes are compatible with a successful colinker incorporation. These results suggest that the dyes can be accommodated without significant steric hindrance, maintaining structural integrity of the 3D network and enabling cosite substitution of conventional linkers.

2. Results and Discussion

2.1. Synthesis of Novel Dyes L0-TA and L1-TA

The two novel organic linkers, **L0-TA** and **L1-TA**, were obtained by introducing a TA terminal moiety into two dye structures commonly reported in the literature of molecular solar devices (**L0** and **L1**). Reference organic dyes **L0** and **L1** have been synthesized, optimizing literature procedures **Scheme 1**.[36,37] To obtain dye **L0**, the brominated triphenylamine **2** was subjected to a selective formylation using *n*-BuLi and DMF, yielding the aldehyde **3**, which was then subjected to a Knoevenagel condensation with cyanoacetic acid to give dye **L0**. Similarly, the preparation of dye **L1** started with a Suzuki–Miyaura cross-coupling between the brominated triphenylamine **2** and 5-formyl-2-thiopheneboronic acid (**4**) to afford the aldehyde **5**, which was then subjected to a Knoevenagel condensation in presence of cyanoacetic acid (**6**) to afford dye **L1**. Subsequently, both dye **L0** and **L1** were submitted to a peptide-like coupling with 2-aminoterephthalic acid (**7**) using 4-(4,6-dimethoxy-1,3,5-triazin-2-yl)-4-methylmorpholinium chloride (DMTMM) and *N*-methylmorpholine (NMM) as coupling agents to afford the desired products **L0-TA** and **L1-TA**. All the intermediates have been investigated by ^{1}H-NMR spectroscopy (Figures S1–S4, Supporting Information), while the two novel dyes **L0-TA** and **L1-TA** have been fully characterized through ^{1}H-NMR, ^{13}C-NMR spectroscopy, and ESI-Mass spectrometry. The synthesis and characterization details are provided in the Experimental Section and in Figures S5–S10, Supporting Information.

2.2. Optical and Electrochemical Characterization of Dyes

To validate the suitability of the new dyes in MOF systems, a detailed spectroscopic and electrochemical characterization

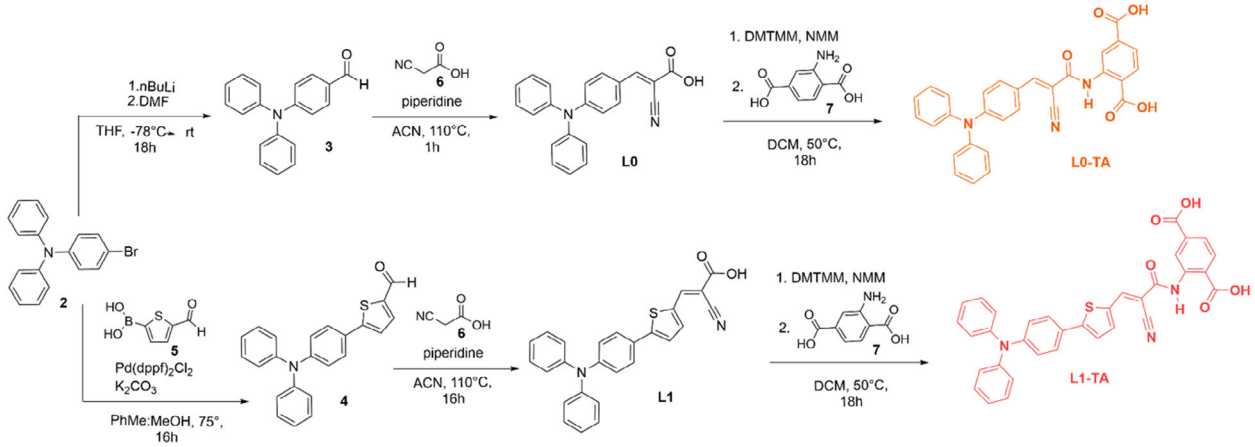

Scheme 1. Synthetic pathway for the synthesis of dyes **L0-TA** and **L1-TA**.

Research Article
doi.org/10.1002/cmtd.202500124
Chemistry Europe
European Chemical Societies Publishing

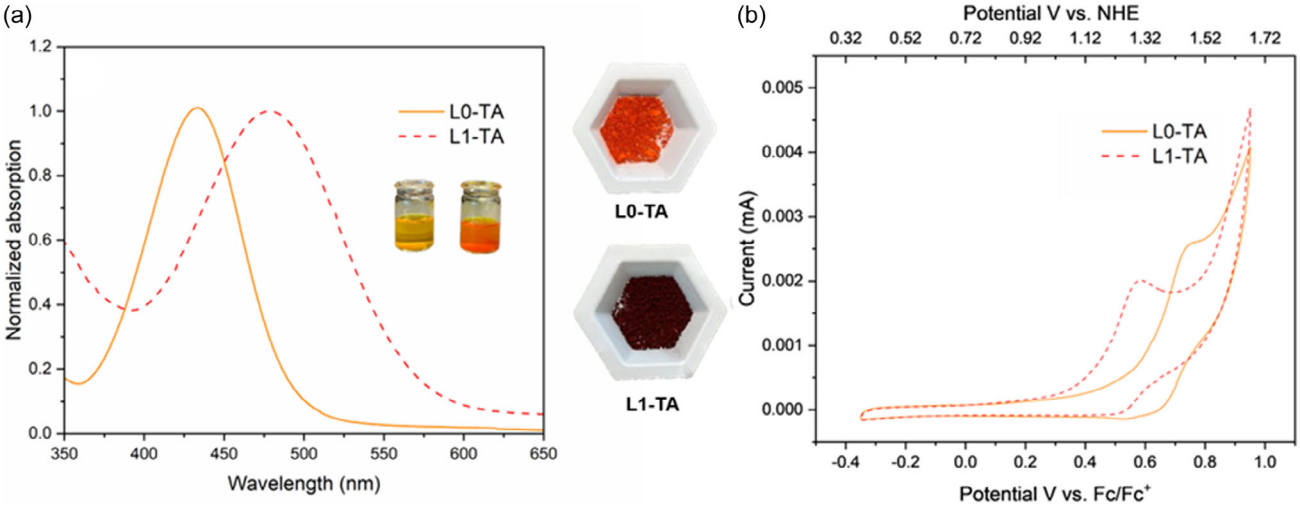

Figure 2. a) Normalized UV−vis absorption spectra of dyes **L0-TA** (orange solid line), **L1-TA** (red solid line), in a 0.05 M acetone solution. b) CV of **L0-TA** and **L1-TA**, 10−5 M solution in DMF with 0.1 M N $(n\text{-Bu})_4ClO_4$.

was carried out. The UV–vis spectra of both dyes recorded in acetone present an intense ICT band in the 350–550 nm region and a molar extinction coefficient (ε) in the range of 12,000–14,000 (M^{-1} cm^{-1}) (Table S1, Supporting Information, **Figure 2**a). Optical bandgap has been evaluated by means of Tauc plots. The cyclic voltammetry (CV) of the dyes, recorded in DMF (Figure 2b), showed a partially reversible behavior at oxidative potentials (potential $>$ 0 V vs. Fc/Fc+). Differential pulse voltammetry (DPV) (Figure S11, Supporting Information) was preferred to determine the oxidation potentials (E_{ox}) and, thus, to calculate the HOMO energy levels. The calculated LUMO level for all dyes has been estimated from the corresponding HOMO energy and energy gaps assuming negligible exciton-binding effects, a common approximation when the reduction process is not experimentally observed. All calculated values are listed in Table S1, Supporting Information.

The combination of UV spectra and calculated HOMO and LUMO energy levels of **L0-TA** and **L1-TA** (well aligned with the redox potentials for proton reduction and water oxidation) demonstrates the suitability of both dyes to act as photosensitizing linkers in MOF-based photocatalytic systems.

2.3. Crystallographic Simulations

The feasibility of incorporating **L0-TA** and **L1-TA** as organic linkers within the MIL-125 framework was assessed by crystallographic simulations through simulated annealing (SA) calculations. This stochastic optimization method is usually applied to determine the crystal structure from X-ray powder diffraction (XRPD) profiles. An initial structural model is described in terms of internal and external degrees of freedom and the position and configuration in best agreement with experimental data is found by applying a SA procedure. Here we have applied the same procedure to explore the configurational space of the dye molecules once covalently bound to the aromatic ring of the MOF linker, thus reproducing their role as pendant functional units. By sampling different orientations and conformations of the pendant dyes, the SA procedure provided a set of low-energy solutions that reflect the steric compatibility of each dye with the surrounding framework. In this new procedure, the XRPD profile of the MOF was used considering only the first peaks (green line in **Figure 3**a), to introduce a low-resolution constraint and stereochemical restraints were used to predict the possible spatial orientation of the guest molecules within the MIL-125 porous framework. Therefore, they can also assess the compatibility of the dye molecules with the MOF. Results showed that both dyes can be incorporated as pendant groups in the MIL-125 framework, extending into the porous space and retaining structural flexibility even when covalently bound to a linker molecule. Results of SA simulations are shown in **Figures** 3 and **4**. Figure 3b shows the best nine solutions ranked according to the final cost function values, revealing non-negligible differences among different solutions, which are greater for **L1-TA** (orange bars) than for **L0-TA** (blue bars). This can be interpreted by considering that the incorporation of both dyes leads to energetically stable solutions, with noticeable differences in the cost function values. The more complex structure of **L1-TA** with respect to **L0-TA** gives more sensitivity to the conformational sampling to this compound. Moreover, **L1-TA** reaches the overall lowest-cost solution (rank 1), indicating a better steric compatibility with the MIL-125 framework compared to **L0-TA**. The distribution of cost function values, confined to a narrow range (493.4–494.5), suggests that both molecules can be incorporated as pendant groups within the MOF structure without compromising overall stability. However, the differences observed among the solutions highlight the non-negligible influence of dye orientation and conformation on structural accommodation. The presence of multiple energetically close solutions further emphasizes the conformational flexibility of the system, which can place the pendant substituents in different spatial arrangements while remaining compatible with the MIL-125 framework.

Research Article
doi.org/10.1002/cmtd.202500124
Chemistry Europe
European Chemical Societies Publishing

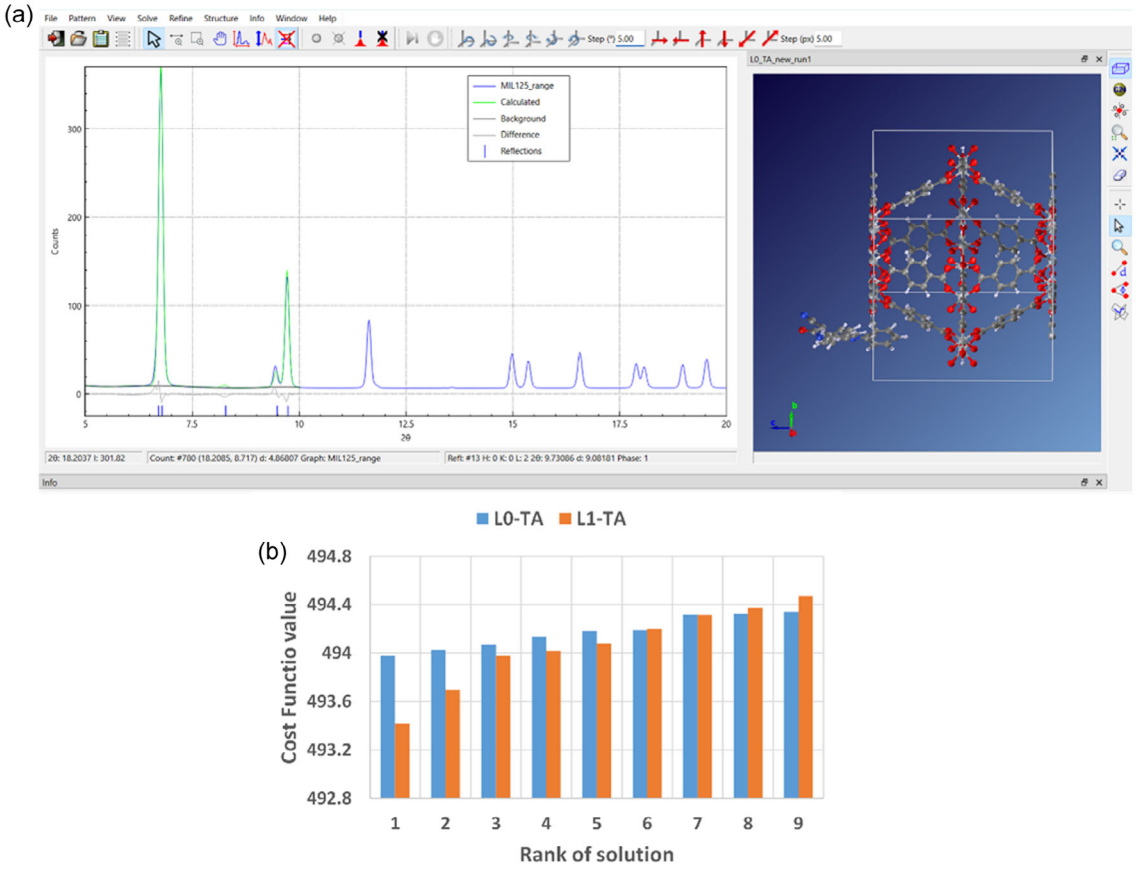

Figure 3. a) Screenshot of the graphic user interface of the EXPO program,[43] showing the measured (blue line), calculated (green line) and difference (gray line) X-ray diffraction profiles and the structural model obtained at the end of the first SA run horizontal bars along the 2J axis indicate the position of the MIL-125 reflections. b) Cost function values for the first nine SA solutions obtained by adding **L0-TA** and **L1-TA** to the MIL-125.

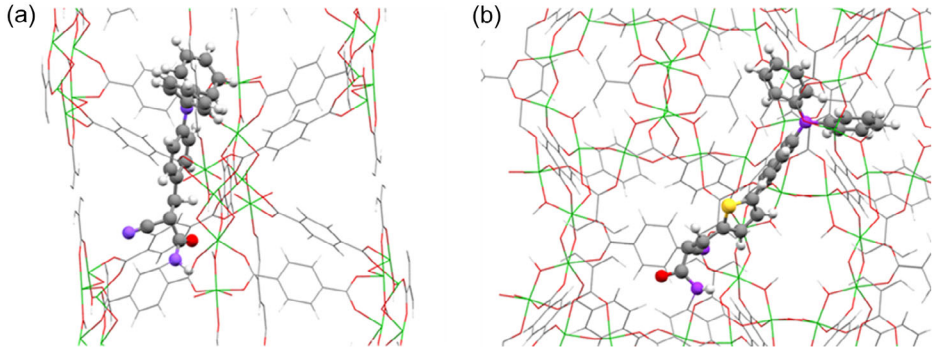

Figure 4. Best solutions obtained by SA for the dye molecule **L0-TA** a) and **L1-TA** b) to the MIL-125 MOF. Dye molecules and MOF are shown in Ball and Stick and Wireframe representation, respectively. Titanium, sulfur, oxygen, nitrogen, carbon, and hydrogen atoms are shown in green, yellow, red, purple, gray, and light gray, respectively.

The best SA configurations of **L0-TA** (a) and **L1-TA** (b) when covalently attached as pendant linkers to the MIL-125 framework are depicted in Figure 4. Both dyes can be accommodated without any atomic clashes, maintaining a realistic binding geometry with the aromatic linker. The comparison highlights that, despite its larger size, **L1-TA** also fits within the steric environment of the MOF, confirming the structural feasibility of both functionalization. A structural comparison among the best nine solutions of each SA simulation (Figures S12 and S13, Supporting Information) highlights that the difference among solutions of the same MOF-dye system lies in the diverse configuration of the dye molecule within the MOF, and that all sampled configurations have no clash with the MOF atoms. Thus, the differences observed for the values of the cost function (Figure 3b) are determined by different arrangements of the dye molecules.

In summary, SA results show that **L0-TA** and even the longer **L1-TA** are both able to bind to the MOF linker according to the imposed constraint and have enough space within the MOF voids to sample their internal flexibility, by adopting different conformations. Besides the conformational heterogeneity showed by the dye with a fixed bond to the MOF, a further structural heterogeneity should be considered by assuming that the dye can equivalently bound to each the four C atoms of the benzene ring of the organic linker of the MOF bound to a hydrogen atom. Based on these arguments, it can envisage that the real crystals of both the MIL-125 + **L0-TA** and MIL-125 + **L1-TA** systems can be affected by static (other than dynamic) disorder related to the dye molecule. In other words, this latter can occupy the crystal unit cells in a different conformation and bound to a different MOF atom. In these conditions, it is very likely that the diffraction signal from the dye molecule is too weak to be detected. Referring to the structural solutions obtained, the expected molecular mass of MIL-125 + **L0-TA** and MIL-125 + **L1-TA** is respectively 8.2% and 9.4% higher than that of the MOF. These values represent the doping level that can be reached for the dye in the MOF, which should correlate to the photophysical properties expected for the material.

3. Conclusion

In this work, two novel functionalized organic linkers, **L0-TA** and **L1-TA**, based on D–π–A structures, were successfully synthesized to integrate vis-light absorption capabilities into MOFs. Spectroscopic and electrochemical studies confirmed that both compounds exhibit intense ICT bands and energy levels suitable for efficient electron transfer, making them promising candidates for photocatalytic hydrogen production. Crystallographic simulations demonstrated the structural compatibility of the new linkers with the MIL-125 framework, showing that both **L0-TA** and **L1-TA** can be incorporated as colinkers without inducing significant steric hindrance.

Despite the relatively large size of these chromophores, their combination with conventional TA linkers can preserve MOF crystallinity while enhancing light-harvesting properties. Overall, this study highlights that the design of functionalized D–π–A linkers represents an effective strategy to expand MOF functionality and improve the performance of vis-light-driven photocatalysis, paving the way for new hybrid materials for sustainable and efficient hydrogen production via solar energy.

Experimental Section

General Information

The starting reagents, obtained from commercial suppliers at the highest purity grade, were used without further purification. Anhydrous solvents, sourced from Sigma–Aldrich, were also used as received. NMR spectra were recorded with a Bruker Avance Neo spectrometer operating at 400 MHz (^{1}H) and 101 MHz (^{13}C). Coupling constants are given in Hz. Flash chromatography was performed with Merck grade 9385 silica gel 230–400 mesh (60 A). Reactions performed under an inert atmosphere were performed in oven-dried glassware, and a nitrogen atmosphere was generated with the Schlenk technique. The conversion was monitored by thin-layer chromatography using UV light (254 and 365 nm) as a visualizing agent. Absorption spectra were recorded with a V-570 Jasco spectrophotometer.

Synthesis of 4-(*N*,*N*-Diphenylamino)benzaldehyde (3)

To a solution of 4-bromotriphenylamine (**2**) (0.634 g; 1.96 mmol; 1 eq) in anhydrous THF (10 mL), at −78 °C, under inert atmosphere, *n*-BuLi (1.6 M in hexane) (1.83 mL; 2.93 mmol; 1.5 eq) was added. After 30 min of vigorous stirring, anhydrous DMF (0.214 g; 2.93 mmol; 1.5 eq) was added. The reaction mixture was left warming to rt overnight. The mixture was then quenched with H_2O and diluted with AcOEt. The organic phase was washed with H_2O (2 × 100 mL). The combined organic phase was dried over Na_2SO_4 and filtered. Concentration under reduced pressure of the solvent gave the crude product that was purified through flash column chromatography (silica gel heptane:-dichloromethane ((DCM) 10:1) to obtain the desired product **3** as a yellow solid in 43% yield (0.228 g; 0.83 mmol). ^{1}H NMR (400 MHz, $CDCl_3$) δ 9.81 (s, 1H), 7.67 (d, J = 8.8 Hz, 2H), 7.34 (t, J = 7.7 Hz 4H), 7.18–7.16 (m, H), 7.00 (d, J = 8.8 Hz, 2H).[37,38]

Synthesis of 4-thiophene-2-carbaldehyde Triphenylamine (5)

In a Schlenk tube under an inert atmosphere, an anhydrous solution of 4-bromotriphenylamine (**2**) (1.282 g, 3.95 mmol, 0.75 eq) in a mixed solvent of MeOH/PhMe (1:1, 40 mL) was prepared. 5-Formyl-2-thiopheneboronic acid (**4**) (0.822 g, 5.27 mmol, 1.33 eq), Pd(dppf)Cl_2 (0.039 g, 0.055 mmol, 0.014 eq), and K_2CO_3 (2.80 g, 20.25 mmol, 5.13 eq) were then added to the tube. The mixture was maintained at 75 °C overnight under an inert atmosphere (N_2). After 16 h, the reaction mixture was diluted with AcOEt and extracted with water (3 × 20 mL). The organic phase was isolated, dried over Na_2SO_4, filtered, and concentrated under reduced pressure. The crude product was purified by column chromatography (from heptane and followed by a gradient of AcOEt:DCM 10:1, 5:1, 1:1). The fractions containing the desired product were combined and concentrated to give a light-yellow solid (**5**) in 52% yield (0.732 g; 2.06 mmol). ^{1}H NMR (400 MHz, $CDCl_3$) δ 9.85 (s, 1H), 7.70 (d, J = 4.0 Hz, 1H), 7.5 (d, J = 8.7 Hz, 2H), 7.32–7.28 (m, 5H), 7.12–7.05 (m, 8H).[36]

Synthesis of L0

To a solution of 4-(*N*,*N*-Diphenylamino)benzaldehyde (**3**) (0.228 g; 0.83 mmol; 1 eq) in 30 mL of anhydrous ACN under inert atmosphere, piperidine (0.49 mL; 4.98 mmol; 6 eq) and cyanoacetic acid (**6**) (0.353 g; 4.15 mmol; 5 eq) were added. The reaction mixture was refluxed for 1 h. The mixture was then diluted with DCM, and the organic phase was washed with H_2O (2 × 50 mL). The combined organic phase was dried over Na_2SO_4 and filtered. Concentration under reduced pressure of the solvent gave the crude product that was purified through flash column chromatography (silica gel AcOEt) to obtain the desired product **L0** as an orange solid in 98% yield (0.265 g; 0.78 mmol). ^{1}H NMR (400 MHz, $CDCl_3$) δ 8.13 (s, 1H), 7.87 (d, J = 9.00 Hz, 2H), 7.37 (t, J = 7.5 Hz, 4H), 7.23–7.19 (m, 6H), 6.96 (d, J = 9.00 Hz, 2H).[36]

Synthesis of L1

To a solution of 4-thiophene-2-carbaldehyde triphenylamine (**4**) (0.670 g; 1.89 mmol; 1 eq) in 50 mL of anhydrous ACN under inert

atmosphere, piperidine (1.3 mL; 13.16 mmol; 7 eq) and cyanoacetic acid (**6**) (0.970 g; 11.41 mmol; 6 eq) were added. The reaction mixture was refluxed overnight. The mixture was then diluted with DCM, and the organic phase was washed with H_2O (2 x 100 mL). The combined organic phase was dried over Na_2SO_4 and filtered. Concentration under reduced pressure of the solvent gave the crude product that was purified through flash column chromatography (silica gel DCM:MeOH 10:1) to obtain the desired product **L1** as an orange solid in 79% yield (0.634 g; 1.50 mmol). ^{1}H NMR (400 MHz, DMSO-d_6) δ 8.16 (s, 1H), 7.74 (d, $J = 4.0$ Hz, 1H), 7.62 (d, $J = 8.7$ Hz, 2H), 7.52 (d, $J = 4.0$ Hz, 1H), 7.35 (t, $J = 7.7$ Hz, 4H), 7.14–7.08 (m, 6H), 6.97 (d, $J = 8.7$ Hz, 2H).[36]

Synthesis of L0-TA

To a solution of dye **L0** (0.488 g; 1.49 mmol; 1 eq) in anhydrous DCM (50 mL), under inert atmosphere, DMTMM (0.494 g; 1.78 mmol; 1.2 eq) and NMM (0.25 mL; 0.226 g; 2.22 mmol; 1.5 eq) were added. After 15 min of stirring, 2-aminoterephthalic acid (**7**) (0.810 g; 4.47 mmol; 3 eq) was added. The reaction mixture was stirred at 50 °C overnight. The mixture was then diluted with DCM, and the organic phase was washed with an aqueous solution of Na_2CO_3 (pH $\simeq$ 10) (5 $\times$ 100 mL) and an aqueous HCl solution (pH $\simeq$ 3). The combined organic phase was dried over Na_2SO_4 and filtered. Concentration under reduced pressure of the solvent gave the crude product that was purified through flash column chromatography (silica gel AcOEt:AcOH 400:1) to obtain the desired product **L0-TA** as an orange solid in 70% yield (0.708 g; 1.41 mmol). ^{1}H NMR (400 MHz, DMSO-d_6) δ 9.21 (s, 1H), 8.25 (s, 1H), 8.11 (d, $J = 8.2$ Hz, 1H), 7.93 (d, $J = 9$ Hz, 2H), 7.72 (d, $J = 9.5$ Hz, 1H), 7.43 (t, $J = 7.9$ Hz, 4H), 7.26–7.22 (m, 7H), 6.88 (d, $J = 8.9$ Hz, 2H). ^{13}C NMR (101 MHz, DMSO-d_6) δ 169.5, 167.0, 160.5, 153.8, 152.2, 145.7, 140.9, 133.4, 133.3, 131.9, 130.5, 127.0, 126.2, 124.2, 123.6, 123.4, 121.5, 118.7, 118.6, 117.2. Elemental analysis calculated (%) for $C_{30}H_{21}N_3O_5$: C, 71.56; H, 4.20; N, 8.35; found C 71.87; H 4.9; N 7.83 m/z: $[M+H]^-$ calculated for C30H20N3O5 502.1403, found 502.1405.

Synthesis of L1-TA

To a solution of dye **L1** (0.450 g; 1.06 mmol; 1 eq) in anhydrous DCM (50 mL) under inert atmosphere, NMM (0.35 mL; 3.20 mmol; 3 eq) and DMTMM (0.588 g; 2.12 mmol; 2.0 eq) were added. After 15 min of stirring, 2-aminoterephthalic acid (**7**) (0.967 g; 5.32 mmol; 5 eq) was added. The reaction mixture was stirred at 50 °C overnight. The mixture was then diluted with DCM, and the organic phase was washed with a solution of Na_2CO_3 (pH $\simeq$ 10) (5 $\times$ 100 mL). The combined organic phase was dried over Na_2SO_4 and filtered. Concentration under reduced pressure of the solvent gave the crude product that was purified through flash column chromatography (silica gel AcOEt:AcOH 200:1) to obtain the desired product **L1-TA** as a red solid in 18% yield (0.112 g; 0.19 mmol). ^{1}H NMR (400 MHz, DMSO-d_6) δ 9.17 (s, 1H), 8.50 (s, 1H), 8.11 (d, $J = 8.1$ Hz, 1H), 7.98 (d, $J = 4.0$ Hz, 1H), 7.67 (d, $J = 8.7$ Hz, 3H), 7.63 (d, $J = 4.0$ Hz, 1H), 7.36 (t, $J = 7.6$ Hz, 4H), 7.15–7.09 (m, 7H), 6.96 (d, J = 8.7 Hz, 2H). ^{13}C NMR (101 MHz, DMSO-d_6) δ 169.5, 167.2, 160.1, 153.3; 149.2, 146.8, 145.2, 141.8, 140.8, 134.3, 131.8, 130.4, 127.9, 125.8, 125.5, 124.7, 124.5, 124.0, 122.1, 121.1, 116.8, 100.2. Elemental analysis calculated (%) for $C_{34}H_{23}N_3O_5S$ C, 69.73; H, 3.96; N, 7.18; found C 70.1; H 3.69; N 7.95 m/z: $[M+H]^-$ calculated for C34H22N3O5S 584.1280, found 584.1285.

Methods: Electrochemical Characterization

CV was carried out at a scan rate of 50 mV s^{-1}, using a Bio-logic SP-240 potentiostat in a three-electrode electrochemical cell under nitrogen. The working, counter, and pseudo reference electrodes were a glassy carbon working electrode (surface area = 0.08 cm^2), Pt wire and an Ag/Ag^+ TBAP in CH_3CN (0.1 M tetrabutylammonium perchlorate and 0.01 M $AgNO_3$ in acetonitrile) in a 0.1 M $TBAClO_4$ solution in DMF. The same setup was used for DPV, recorded at a pulse width of 50.0 ms, a stop height of 10 mV, a step time of 500 ms of 20 mV s^{-1}, and a pulse height of 2.5 mV. The Pt wire was sonicated for 15 min in deionized water, washed with 2-propanol, and cycled for 50 times in 0.5 M H_2SO_4 before use. The Ag/Ag^+ pseudoreference electrode was calibrated by adding ferrocene (10^{-3} M, Fc) to the test solution after each measurement.

Methods: ESI Mass Spectrometry

Samples were dissolved in acetonitrile at a concentration of 1 mg/mL, then diluted 1:1000 in 50% ACN containing 0.1% formic acid, centrifuged, and analyzed. Spectra were acquired on a hybrid quadrupole time-of-flight mass spectrometer (Xevo G2-XS, Waters Corporation, Milford, MA, USA). Full scan analyses were performed over the *m/z* range 50–1200 at a scan rate of 0.1 spectra/s in negative ionization mode. Additional MS settings were as follows: capillary voltage 3 kV; sampling cone 40 V; source temperature 120 °C, desolvation temperature 350 °C, desolvation gas at 1000 L h^{-1} at 550 °C; cone gas flow at 30 L h^{-1}. Data were acquired with MassLynx software (version 4.2, Waters Corporation, Milford, MA, USA). Leucine enkephalin 200 pg ml^{-1} dissolved in 50% ACN in water containing 0.1% formic acid was acquired at 10 s intervals during runs for lock mass correction of data.

Methods: Preparation of Structural Models

The CIF file of the structural model of the MOF MIL-125 (CCDC 751,157) was preliminarily processed using Mercury software.[39] First any solvent molecule was deleted, then the full unit cell was populated by applying the crystallographic symmetry (I 4/m m m) and finally the structure was converted to the P 1 space group. The original symmetry of the MOF was not applied during the simulation, as the dye molecule accommodate in a preformed MOF structure, and the high number of symmetry operators would require the simultaneous addition of multiple molecules in each unit cell, often resulting in overlapping configurations. A further structural modification involved the removal of a hydrogen atom bonded to a carbon atom on the benzene ring of TA, which is the organic linker in the MOF framework. This modification was applied to allow the covalent bond between the nitrogen atom of the amide group of the dye molecule (**L0-TA** or **L1-TA**) with a given carbon of the TA, which constitutes the framework linker. This procedure is crucial for studying the orientation of the dye within the structure and the availability of porous space. The dye molecules were drawn using ChemSketch[40] and then converted into CIF format. Both are asymmetric.

Metehods: X-Ray Diffraction Data Collection

The high-resolution X-ray powder diffraction pattern of MIL-125 was collected at the synchrotron European Synchrotron Radiation Facility on beamline BM31. It was equipped by a PILATUS3 X CdTe 2 M detector, which was positioned 889 mm from the sample, put in a glass capillary of 0.5 mm diameter. Two consecutive measurements of 30 s each were carried out. They were performed in transmission mode at room temperature, with an energy of 48.7 keV ($\lambda = 0.25448$ Å). A Si standard was also measured for calibration. The two diffraction images acquired were merged, masked, and integrated azimuthally by using the software Bubble.[41]

Methods: Simulated Annealing Procedure

Powder diffraction data measured for MIL-125[42] and the preprocessed structural files of the MOF and the two dye molecules **L0** and **L1** were used as input files for SA runs performed by using EXPO,[43] a software dedicated to the structure determination from powder diffraction data. Two simulations were performed with the same protocol, by using the following input files: the MIL-125 powder diffraction profile and CIF file and the CIF files for **L0-TA** and **L1-TA**, respectively. In each simulation, the initial SA temperature was set to 10 (arbitrary units), then progressively decreased to facilitate exploration of the solution space and avoid local minima. The MOF structure was considered fixed, while the dye molecule was treated as free to move and flexible. The number of internal degrees of freedom identified for **L0-TA** and for **L1-TA** was 31 and 32, respectively. The crystallographic weighted profile agreement factor (R_{wp}) was chosen as cost function, which measured the similarity between observed and calculated profile. Antibump restraints were applied to prevent the molecule from overlapping with itself or with the MOF. In addition, a distance restraint was applied between two selected atoms of the fragments. Specifically, 1.42 ± 0.03 Å (weight 10,000) was imposed between the N atom of the dye amide group and one of the four C atoms of the benzene ring of the organic linker of the MOF bound to a hydrogen atom. The overall formula of the cost function is the following

$$\mathrm{CF} = \sqrt{\frac{\sum_i w_i \left(y_i^{\mathrm{obs}} - y_i^{\mathrm{calc}}\right)^2}{\sum_i w_i \left(y_i^{\mathrm{obs}}\right)^2} + \sum_{ij} w_{ij} \left(d_{ij}^{\mathrm{min}} - d_{ij}^{\mathrm{model}}\right)^2 + w_{\mathrm{NO}} \left(d_{\mathrm{NC}}^{\mathrm{ref}} - d_{\mathrm{NC}}^{\mathrm{model}}\right)^2} \quad (1)$$

where y_i^{obs} and y_i^{calc} are the intensities of the observed and calculated XRPD profile at *i*-th experimental step, respectively, and $w_i = 1/y_i^{\mathrm{obs}}$ is the statistical weight. The second and third terms correspond to geometric restraints, which penalize unrealistically short interatomic distances and maintain a covalent bond distance among between a selected atoms of the guest molecule and the MOF framework, respectively. In the antibump term, d_{ij}^{min} and d_{ij}^{model}, with the condition $d_{ij}^{\mathrm{min}} > d_{ij}^{\mathrm{model}}$, are the minimum ideal distances and the model distances, respectively, between pairs of atoms *i* and *j*, and summation is over all the possible contacts between atoms of the molecule and one atom of the molecule and one atom of the MOF. d_{ij}^{min} is the sum of the atomic radii of atoms *i* and *j* multiplied by a scale factor. In the distance term $d_{\mathrm{NC}}^{\mathrm{ref}}$ and $d_{\mathrm{NC}}^{\mathrm{model}}$ are the reference (1.42 Å) and current values of the distance between the above-described N and C atoms, and w_{NO} is the associated weight (1000). The SA algorithm explores the configurational space by minimizing this cost function through stochastic sampling governed by Metropolis acceptance criteria.

To improve the reliability of the simulation process, a resolution limit of 8.8 Å, corresponding to $2\theta = 2.0°$, was applied to the X-ray powder diffraction profile to calculate the cost function, thus only selecting three low-resolution peaks, corresponding to reflections (110), (300), and (421). In direct space, this strategy results in using a molecular envelope defined by a low-resolution view of the MOF to drive more efficiently the SA algorithm toward minima. On the other hand, the exclusion of high-resolution reflections avoids bias due to the absence of any dye molecule in the measured sample, and at the same time minimizes the impact of experimental noise. A total of 30 SA cycles were performed, each of them with different initial conditions, to increase the probability of finding the final solution. At the end of the simulation, the nine best structural models were selected.[43]

Supporting Information

The authors have cited additional references within the Supporting Information.

Acknowledgements

The authors thank the Ministero dell'Università e della Ricerca (PRIN2022 Mendeleev, Project no. 2022KMS84P funded by European Union—NextGenerationEU, Piano Nazionale di Ripresa e Resilienza (PNRR) M4 C2 I.1.1 CUP H53D23004590006), Ministero dell'Ambiente e della Sicurezza Energetica (SOLE-H2, Project RSH2A_000004—CUP: F57G25000080006, funded by European Union—NextGenerationEU, Piano Nazionale di Ripresa e Resilienza (PNRR) Missione 2 Componente 2 Investimento 3.5—D.D. 279 05/08/2025, and Sustainable Mobility Center (CNMS-MOST) funded by European Union—NextGenerationEU, Piano Nazionale di Ripresa e Resilienza (PNRR) Missione 4 Componente 2, Investimento 1.4—D.D. 1033 17/06/2022, CN00000023 - CUP:H43C22000510001) for financial support. Open Access publishing facilitated by Università degli Studi di Milano-Bicocca, as part of the Wiley—CRUI-CARE agreement. The authors also acknowledge the European Synchrotron Radiation Facility (ESRF) for provision of synchrotron radiation facilities under proposal number EV-648 and the authors would like to thank Wouter van Beek, Dragos Costantin Stoian, and Kenneth Marshall for assistance and support in using beamline BM31. The authors also thank Roberto Lassandro for help in sample preparation. The BM31 setup was funded by the Swiss National Science Foundation (grant 206021_189629) and the Research Council of Norway (grant 296087).

Conflict of Interest

The authors declare no conflict of interest.

Data Availability Statement

R. Caliandro, C. Favia, R. Lassandro (2028). Structure-based optimization of metal-organic frameworks (MOFs) for green energy applications [MIL-125]. European Synchrotron Radiation Facility. doi.org/10.15151/ESRF-ES-2118292034.

Keywords: D-π-A dyes · light harvesting · metal organic frameworks · organic linkers · photocatalysis

[1] C. W. Jones, *JACS Au.* **2022**, *2*, 1504.
[2] R. U. Rajesh, T. Mathew, H. Kumar, A. Singhal, L. Thomas, *Inorg. Chem. Commun.* **2024**, *162*, 112223.
[3] C. Jiang, X. Wang, Y. Ouyang, K. Lu, W. Jiang, H. Xu, X. Wei, Z. Wang, F. Dai, D. Sun, *Nanoscale Adv.* **2022**, *4*, 2077.
[4] W.-T. Koo, J.-S. Jang, I.-D. Kim, *Chem* **2019**, *5*, 1938.
[5] H. Li, L. Li, R.-B. Lin, W. Zhou, Z. Zhang, S. Xiang, B. Chen, *EnergyChem* **2019**, *1*, 100006.
[6] D. Yang, B. C. Gates, *ACS Catal.* **2019**, *9*, 1779.

[7] L. Jiao, H.-L. Jiang, *Chin. J. Catal.* **2023**, *45*, 1.
[8] O. Bettucci, G. Salerno, N. Manfredi, A. Abbotto, *Tetrahedron Green Chem.* **2024**, *3*, 100040.
[9] C. Zhang, Y. Wu, D. Li, H.-L. Jiang, *Chem. Sci.* **2025**, *16*, 13149.
[10] D. A. Reddy, Y. Kim, M. Gopannagari, D. P. Kumar, T. K. Kim, *Sustain. Energy Fuels* **2021**, *5*, 1597.
[11] S. Navalón, A. Dhakshinamoorthy, M. Álvaro, B. Ferrer, H. García, *Chem. Rev.* **2023**, *123*, 445.
[12] Y. Fu, D. Sun, Y. Chen, R. Huang, Z. Ding, X. Fu, Z. Li, *Angew. Chem. Int. Ed.* **2012**, *51*, 3364.
[13] L. Lu, B. Wu, W. Shi, P. Cheng, *Inorg. Chem. Front.* **2019**, *6*, 3456.
[14] K. Zhang, H. Hu, L. Shi, B. Jia, H. Huang, X. Han, X. Sun, T. Ma, *Small Sci.* **2021**, *1*, 2100060.
[15] Z. M. Soilis, T. H. Choi, J. Brennan, R. R. Frontiera, J. K. Johnson, N. L. Rosi, *Chem. Mater.* **2024**, *36*, 1773.
[16] M. E. Foster, J. D. Azoulay, B. M. Wong, M. D. Allendorf, *Chem. Sci.* **2014**, *5*, 2081.
[17] M. A. Nasalevich, M. G. Goesten, T. J. Savenije, F. Kapteijn, J. Gascon, *Chem. Commun.* **2013**, *49*, 10575.
[18] Y. Qin, M. Hao, D. Wang, Z. Li, *Dalton Trans.* **2021**, *50*, 13201.
[19] H. Lin, Y. Xu, B. Wang, D.-S. Li, T. Zhou, J. Zhang, *Small Struct.* **2022**, *3*, 2100176.
[20] Y.-F. Chen, L.-L. Tan, J.-M. Liu, S. Qin, Z.-Q. Xie, J.-F. Huang, Y.-W. Xu, L.-M. Xiao, C.-Y. Su, *Appl. Catal. B- Environ.* **2017**, *206*, 426.
[21] S. Yang, W. Liu, Y. Zhang, X. Jia, J. Sun, C. Zhang, M. Liu, *J. Mater. Chem. A* **2024**, *12*, 28161.
[22] O.-Y. Yang, X.-J. Gao, G.-D. Qi, Y. Wang, W.-W. Dong, Z.-F. Tian, J. Zhao, D.-S. Li, Q. Zhang, *ACS Appl. Energy Mater.* **2023**, *6*, 334.
[23] P. Verma, R. V. Singh, A. M. Banerjee, M. R. Pai, *Int. J. Hydrogen Energy* **2025**, *107*, 569.
[24] H. Hintz, S. Wuttke, *Chem. Commun.* **2014**, *50*, 11472.
[25] P. Narea, I. Brito, Y. Quintero, E. Camú, *Int. J. Mol. Sci.* **2024**, *25*, 199.
[26] C. Delacourt, J.-P. Goddard, A. Spangenberg, M. Cormier, *ChemPhotoChem* **2025**, *9*, e202400370.
[27] T. Ceper, D. Costabel, D. Kowalczyk, K. Peneva, F. H. Schacher, *ACS Appl. Mater. Interfaces* **2024**, *16*, 24796.
[28] F.-l. Zeng, Z. Jia, T.-P. Loh, *Adv. Synth. Catal.* **2024**, *366*, 4536.
[29] G. Salerno, O. Bettucci, N. Manfredi, L. Stendardo, E. Veronese, P. Metrangolo, A. Abbotto, *Global Chall.* **2024**, *8*, 2300345.
[30] M. Khalid, M. U. Khan, I. Shafiq, R. Hussain, A. Ali, M. Imran, A. A. C. Braga, M. F. ur Rehman, M. S. Akram, *R. Soc. Open Sci.* **2021**, *8*, 210570.
[31] G. Ersoy, M. Henary, *Biomolecules* **2025**, *15*, 119.
[32] M. Ueda, R. Nagayama, M. Nagaoka, N. Suzuki, S. Kodama, T. Maeda, S.-i. Kato, S. Yagi, *Molecules* **2025**, *30*, 3084.
[33] G. Salerno, D. Franchi, A. Dessì, M. Bartolini, N. Manfredi, A. Abbotto, O. Bettucci, *ChemistryOpen* **2025**, *14*, e202400464.
[34] G. Salerno, B. Cecconi, O. Bettucci, M. Monai, L. Zani, D. Franchi, M. Calamante, A. Mordini, T. Montini, P. Fornasiero, N. Manfredi, A. Abbotto, *Eur. J. Org. Chem.* **2023**, *26*, e202300924.
[35] O. Bettucci, D. Franchi, A. Sinicropi, M. di Donato, P. Foggi, F. F. de Biani, G. Reginato, L. Zani, M. Calamante, A. Mordini, *Eur. J. Org. Chem.* **2019**, *2019*, 812.
[36] D. P. Hagberg, T. Marinado, K. M. Karlsson, K. Nonomura, P. Qin, G. Boschloo, T. Brinck, A. Hagfeldt, L. Sun, *J. Org. Chem.* **2007**, *72*, 9550.
[37] X. Sun, L. Xie, W. Huo, K. Lin, Y. Yang, X. Chi, C. Zhao, F. Zhang, J. Li, D. Xia, J. Zhang, *J. Photochem. Photobiol. A: Chem.* **2025**, *467*, 116450.
[38] C. Li, W. Yang, W. Zhou, M. Zhang, R. Xue, M. Li, Z. Cheng, *New J. Chem.* **2016**, *40*, 8837.
[39] C. F. Macrae, I. Sovago, S. J. Cottrell, P. T. Galek, P. McCabe, E. Pidcock, M. Platings, G. P. Shields, J. S. Stevens, M. Towler, *J. Appl. Crystallogr.* **2020**, *53*, 226.
[40] Z. Li, H. Wan, Y. Shi, P. Ouyang, *J. Chem. Inf. Comput. Sci.* **2004**, *44*, 1886.
[41] V. Dyadkin, P. Pattison, V. Dmitriev, D. Chernyshov, *J. Synchr. Rad.* **2016**, *23*, 825.
[42] R. Caliandro, C. Favia, R. Lassandro, *Structure-Based Optimization of Metal-Organic Frameworks (MOFs) for Green Energy Applications [Dataset]*, European Synchrotron Radiation Facility **2028**, doi.org/10.15151/ESRF-ES-2118292034.
[43] A. Altomare, C. Cuocci, C. Giacovazzo, A. Moliterni, R. Rizzi, N. Corriero, A. Falcicchio, *J. Appl. Crystallogr.* **2013**, *46*, 1231.

Manuscript received: October 3, 2025
Revised manuscript received: November 16, 2025
Version of record online: